Light Metals 2015
Edited by: Margaret Hyland
TMS (The Minerals, Metals & Materials Society), 2015

OBSERVATION OF ANODIC BUBBLE BEHAVIORS USING LABORATORY SCALE TRANSPARENT ALUMINIUM ELECTROLYSIS CELLS

Zhibin Zhao[1,2], Zhaowen Wang[1], Bingliang Gao[1], Yuqing Feng[2], Zhongning Shi[1], Xianwei Hu[1]
[1] School of Material and Metallurgy
Northeastern University, Shenyang 110089, China
[2] Mineral Resources Flagship
CSIRO, VIC 3168, Australia

Keywords: Aluminum electrolysis; Transparent cell; Anodic bubble

Abstract

Laboratory scale transparent aluminum electrolysis cells were used to study anodic bubble behavior, including bubble layer thickness, bubble shape and coverage at the anode bottom surface, and the resultant cell voltage drop in a very similar environment to real industrial cells. The observation was conducted using two transparent cells, one with side-view and the other with a bottom-view cell design. For the side-observation experiment, the evolution of bubble layer thickness and bubble rising process were studied. In the bottom-observation experiment, bubble behavior was investigated on both unslotted and slotted anodes. Cell voltage was simultaneously recorded for a quantitative investigation of its relevance to bubble coverage. It was found that the cell voltage drop is very consistent with bubble coverage, with a high voltage drop corresponding to a high bubble coverage. The coverage of anodic gas bubbles decreases with the increase of current density. These phenomena were observed on unslotted and slotted anodes. The comparison of unslotted anode and slotted anode indicated that the slot significantly reduces the cell voltage drop, voltage drop fluctuations and bubble coverage.

Introduction

In the aluminum electrolysis process, anodic gas bubbles are generated on the anode bottom and are released out of anode edges in a cyclic pattern [1]. The gas bubbles accumulate beneath anodes, affect current distribution, and even cause anode effects at extreme conditions. The presence of bubbles also makes a contribution in energy consumption: the extra voltage drop due to the bubble layer is about 0.15-0.35 V out of the total cell voltage of 4.0-4.6 V [2]. However, the bubble motion is also a significant driver for the circulation of electrolyte, which is important in increasing bath flow, alumina mixing and heat balance. While the presence of bubbles is an inherent phenomenon in the aluminum electrolysis process, a detailed understanding of the bubble dynamics is necessary to quantitatively assess its relevance to cell performance.

Restricted by the high temperature and heavily corrosive environment of the molten salt, studies of industrial cells are very difficult and expensive, particularly for detailed bubble dynamics. A number of substitutive models have been developed to investigate bubble behavior in the past few decades, such as water models [3-8], low temperature electrolysis models [9-12], numerical models [13-16] and laboratory scale transparent aluminum electrolysis cells [17-23].

Despite being an intensive research area, the detailed understanding of bubble behavior is not fully understood. It is necessary to investigate the anodic bubbles similar to a real environment. On this consideration, the laboratory transparent electrolysis cell, also called 'see-through cell', has been developed to observe bubble behavior similar to real electrolytic systems by several research teams.

Haupin [17] employed sapphire windows held in a graphite crucible to 'see' the electrolysis process. This kind transparent cell was limited in high cost and small viewing window. In the same literature, quartz material was used as the sidewall of the crucibles for the first time. A test quartz tube was suspended in an electric furnace with front and back windows [17, 20]. For better viewing, Qiu [18] applied square-shaped quartz crucibles to study the metal fog, anode effect and other electrolysis phenomena, e.g. alumina dissolution. This design of cell was limited in time and current density as metal fog rapidly arose and led an opaque electrolyte. Qiu [19] improved the transparent cell design using double-chamber crucibles by positioning a square-shaped quartz tube inside the quartz crucible. This way, the small tube acted as the cathode chamber and the rest represented the anode chamber. With this design, the generated metal fog was blocked in the cathode chamber. The observational time were significantly increased. Gao [21] further improved the cell design by implementing two chambers in one quartz crucible with a slot at the bottom of the middle wall connecting the two chambers. The cell can be operated more conveniently. Another kind of 'transparent cell', laboratory X-ray radiographic test, was also carried out in this area [22-23]. X-ray passed through the cell, the areas with different dense materials showed different color in the images.

Although the transparent cell can only be operated at laboratory scale, in which the anode size is 1/50th to 1/30th of a typical modern industrial scale anode size, it offers an excellent opportunity to observe bubble behavior close to industrial smelting cells, particularly the detailed bubble growth process in the bath under the anode, known as the 'anode to cathode distance' (ACD).

This paper presents a study in this direction. The evolution of bubble layer thickness in the ACD and bubble rising process along the anode vertical wall have been studied through a side observation; while the bubble shape, and growth process in the ACD have been studied through a bottom observation. The effect of the presence of a slot in the anode has been assessed in terms of bubble coverage and the resultant voltage drop.

Experimental Setup

The experiments were conducted using two transparent cells developed at Northeastern University for different purposes: side observation using a single-chamber crucible cell and bottom observation using a double-chamber crucible cell.

Figure 1 shows the design of the single-chamber cell for side observation. Both the anode and cathode were put in the single chamber crucible, which contained electrolyte. This design was used in early stage studies [18-19, 21]. As the cathode is under the anode, it is not possible to observe the bubble behavior in the ACD. The crucible design was improved using a double-chamber crucible. As shown in Figure 2, the quartz crucible was made of two chambers, with the anode and cathode put into separate chambers. The two chambers were connected through a slot at the bottom of the crucible. The dimension of the double-chamber crucible is given in Figure 3. The slot, 1 mm in height, allows the current to flow from the anode to the cathode. To observe the bubble behavior in the ACD, a new viewing window at the bottom of furnace was opened. In order to show the diagram clearly, the quartz crucible was rotated for 90 degree to show the cross section in Figure 2.

The side observation is an extension of the previous work using a cylindrical anode [21]. The improvement is that the anode was shielded by an alumina tube to avoid the generation of side bubbles. The anode was positioned 10 mm above the cathode. The cathode was a plate with thickness 10 mm, lying on the bottom of a quartz crucible. The electrode rod was shielded by an alumina tube as well. The electrolyte depth was 30 mm and the current density was set to 0.7 A/cm^2. The bubble behavior was recorded by a High Speed Camera (LIGHT NING RDT) with 100 frames per second (FPS) from side viewing window.

For the bottom observation experiment, two rectangular shaped anodes were used to better represent the industrial anode. The effect of slots was studied by opening a longitudinal slot in the anode. The current density was set from 0.3 to 1.3 A/cm^2. An Industrial Camera (MV-VS078FC) was set at the bottom of furnace to capture variations in anodic bubble behaviors on the unslotted anode and slotted anode. The captured speed was 15 FPS. The corresponding cell voltage during electrolysis was recorded in parallel by an Agilent HP34401A Digital Multi Meter. Bubble morphology and cell voltage were recorded simultaneously for the correlations between bubble behaviors and cell voltage drop.

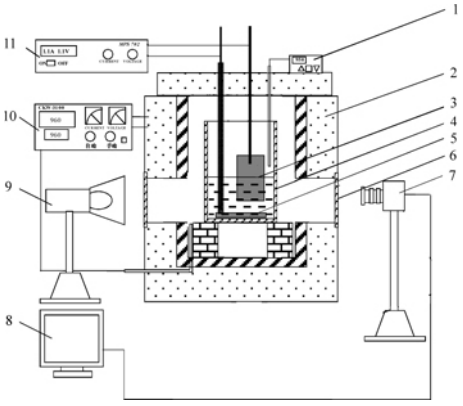

1-Thermocouple; 2-Furnace; 3-Anode; 4-Quartz Crucible; 5-Cathode; 6-Side-view Quartz Window; 7-High Speed Camera; 8-Computer; 9-Light Source; 10-MPS 3100 Temperature Controller; 11-702 DC Power Supply.

Figure 1 The schematic diagram of side-view transparent cell

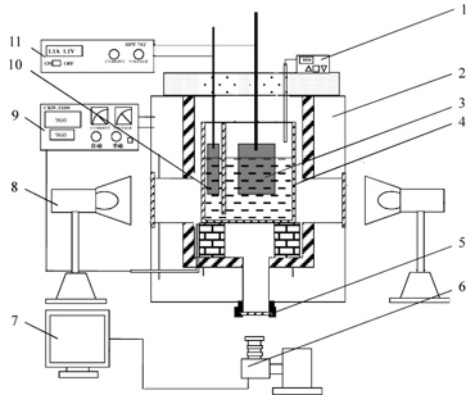

1-Thermocouple; 2-Furnace; 3-Anode; 4-Quartz Crucible; 5-Bottom-view Quartz Window; 6-Industiral Camera; 7-Computer; 8-Light Source; 9-MPS 3100 Temperature Controller; 10-Cathode; 11-702 DC Power Supply.

Figure 2 The schematic diagram of bottom-view transparent cell

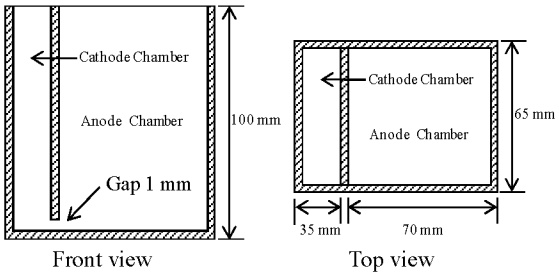

Figure 3 The diagram of double-chambers quartz crucible (wall thickness 3 mm)

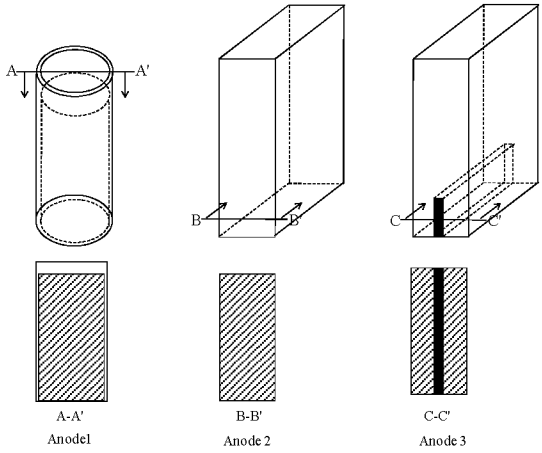

Figure 4 The diagrams of the three kinds of anodes

The geometries of the three kinds of anodes used in this study are described in Figure 4 and Table 1. All anodes and cathodes were made of high-purity graphite.

The composition of the electrolyte used in this experiment was based on a mixture of cryolite (NaF 45.7wt%, AlF_3 41.8wt%, LiF 5wt%, CaF_2 4wt%, Al_2O_3 3.5wt%; CR=2.2). All the compositions were dried at 400℃ for more than 3 hours and stored in a dry container. The furnace temperature was controlled at 950±5℃ by an MPS3100 Temperature Controller.

Table 1 Experiments in this paper

Experiments	Anode	Anode configurations(mm)	Purposes
Side view	Anode 1	Cylinder(ϕ26*50), shielded by an alumina tube	Bubble layer growth and bubble rising in cell channel
Bottom view	Anode 2	Rectangle (22*50)	Bubble behavior in ACD
	Anode 3	Rectangle(22*50*70), with one longitudinal slot (4*15)	The effect of a slot on cell voltage, voltage fluctuation and bubble coverage

Results and Discussion

Bubble Morphologies

Side Observation Using a Side-view Transparent Cell. To record the bubble morphologies clearly, particularly during the bubble rising process, a high speed camera was used.

In a previous study [22], the anode side walls were not insulated; current flowed out of both the sidewall and bottom of the anode. Many bubbles were generated on sidewalls. In this experiment, both anode side walls and the cathode rod were shielded by alumina tubes. This ensures the current flows from anode to cathode vertically. No gas bubbles were generated at the sidewalls of the anode.

Figure 5 shows some characteristic stages in a bubble life cycle. The bubble behavior beneath the anode can be divided into several stages: bubble formation and growth (Figure 5(a)-5(b)); bubble coalescence into a gas layer rapidly (Figure 5(c)); thickness growth of the bubble layer (Figure 5(d)); bubble releasing at the edge of anodes (Figure 5(e)); and bubble rising in side channel (Figure 5(f)-5(h)).

During the bubble formation and growth, individual bubbles can be clearly observed (Figure 5 (b)). Once these bubbles grow to a certain size, they will coalesce to form large bubbles (Figure 5(c)). The bubble expands along the bottom to form a gas layer. It takes about 1.18 s for the gas layer to grow to the maximum thickness, which almost covers the full anode bottom surface (Figure 5(d)). Thereafter, the bubble starts to slide to one side of the anode edge and releases from anode bottom. The bubble attaches to the anode vertical wall when it rises up in the cell channel.

The bubble layer thickness is an important obstacle for reducing the ACD in an industrial operation. In this experiment, the growth of the bubble layer was recorded with the electrolysis time. An averaged value of the whole bubble layer is measured to check its variation with time.

Figure 6 illustrates the variation in averaged gas layer thickness in the ACD with respect to electrolysis time. It is observed that the bubble layer thickness displays cyclical periodic behavior. At some cycles, instead of a smooth growth, the thickness reduces a bit before further growth. Probably, this is attributed to the bubble coalescence effect. When the thickness increases to a maximum value (about 4 mm), it drops suddenly due to the bubble release from the anode edge. This period is referred as a bubble life cycle. The cyclic period varies, ranging from 0.8 to 2 s.

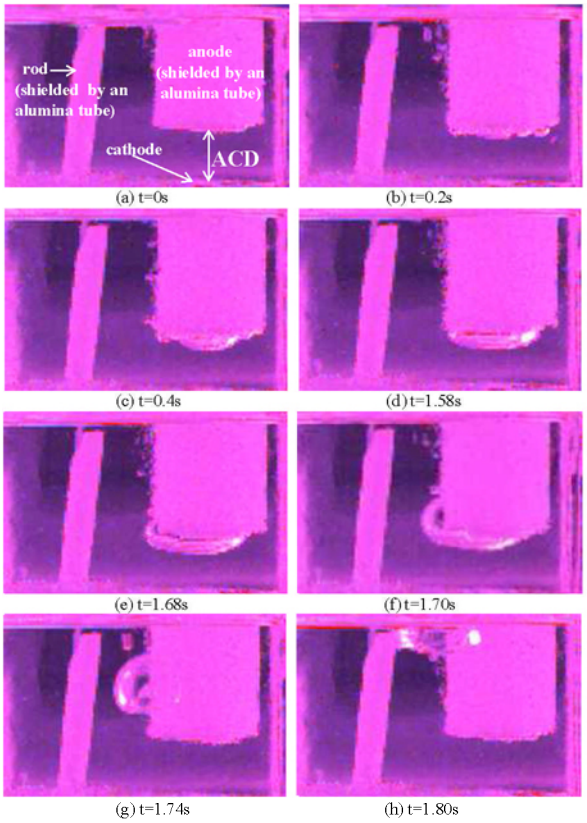

Figure 5 Bubble morphologies in a life cycle

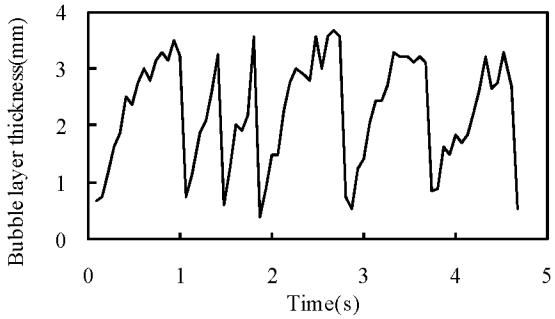

Figure 6 Anodic bubble layer thickness against electrolysis time

Bottom Observation Using a Bottom-view Transparent Cell. The side observation experiment gives a reasonable estimation of the development of bubble layer thickness and the bubble rising process. However, important information, such as bubble shape, bubble coalescence and gas coverage in the ACD, cannot be obtained with this design. With the new design of bottom-view transparent electrolysis cell, the detailed bubble dynamics in the ACD can be observed in detail from bottom of the anode.

In order to capture clear pictures in a long period, an industrial camera was used. As the bubble motion beneath the anode does not change as significantly as bubble rising in cell channels, the industrial camera was capable to capture the bubble characteristics beneath the anode sufficiently.

Figure 7 shows some characteristic stages of the bubble morphologies of an unslotted anode (anode 2 in Figure 4) and a slotted anode (anode 3 in Figure 4) in one life cycle when

current density was 0.9 A/cm^2. The image in the first row in Figure 7 shows the instance right after the release of large bubbles. Some residual bubbles left on the bottom surface can be clearly observed. With the continuation of electrolysis, many small bubbles are generated on the reaction surface. These bubbles continue to grow larger due to gas diffusion. When the bubbles reach a certain size, the edges of some bubbles are connected to form larger bubbles. Some bubbles grow to a size as large as the anode size before they are released from the anode edge.

Figure 7 illustrates the bubble morphologies, which are quite different between unslotted and slotted anodes. The largest bubble size on the slotted anode is much smaller than that on the unslotted anode, as the bubble on the slotted anode cannot cross the slot for further coalescence into big bubbles.

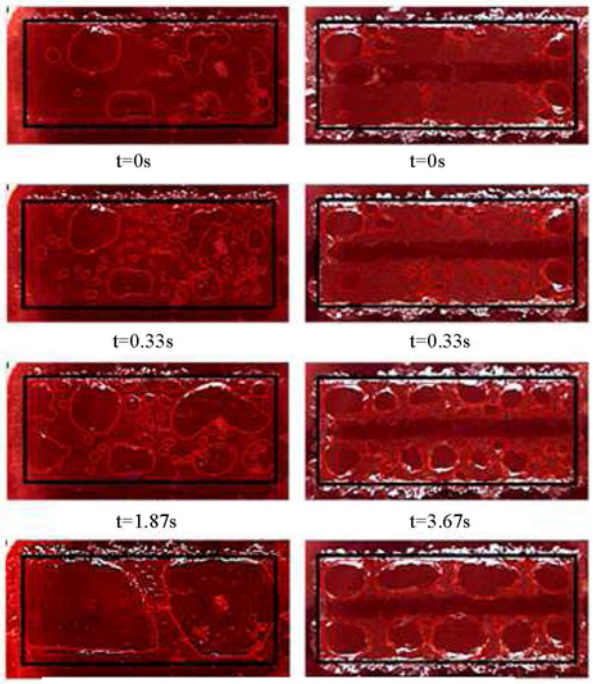

Figure 7 Bubble morphologies in a life cycle on the unslotted anode (a) and slotted anode (b).

The bubble coalescence is believed to be an important source for bubble growth. Figure 8 shows some different bubble coalescence processes for different sized bubbles: Four small and medium sized bubbles coalesce into one bubble in Figure 8(a); Two medium sized bubbles coalesce in Figure 8(b); and two large bubbles coalesce into a bubble which almost cover the whole anode bottom surface. All of the consecutive images were taken at a time interval of 1/15th second. The bubble area increases a bit after the bubble coalescence. This explains why the bubble layer thickness reduces during the bubble growth process shown in Figure 6.

For the selected images showing bubble coalescence, the coalesced bubbles generally maintained their original positions. The recorded video also showed other types of bubble coalescences, e.g. the large bubbles swallow the surrounding small bubbles. More detailed bubble coalescence processes will be discussed in future by further processing of the recorded video.

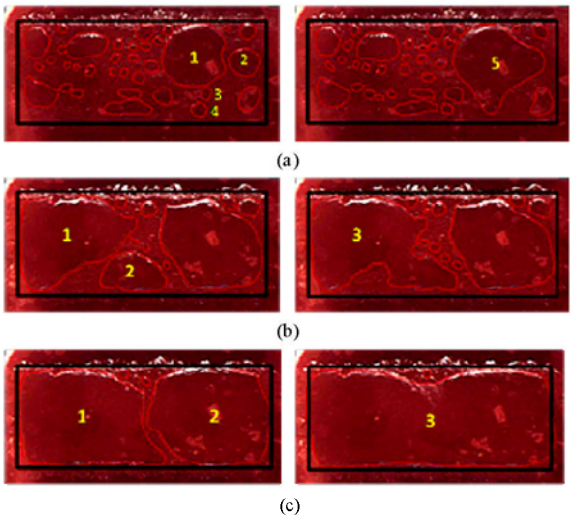

Figure 8 Bubble coalescences for different sized bubbles on the unslotted anode bottom surface at the current density of 0.9 A/cm^2. (a) Small bubble coalescence (b) Medium bubble coalescence (c) Large bubble coalescence

The Effect of Anode Slot

Setting slots on anode bottom is well accepted to be a practical way for energy saving in aluminum electrolysis. In this section, the effect of presence of a longitudinal slot on cell voltage, voltage fluctuation and gas coverage will be discussed.

Cell Voltage Fluctuation. Figure 9 shows the cell voltage drop measured of both unslotted and slotted anodes at the fixed current density of 0.9 A/cm^2. The mean voltage drop is about 6.5 V for the unslotted case. The total current is 18% less for the slotted case at the same current density. If the voltage drop is linearly proportional to the total current, the voltage drop for the slotted case would be 5.33 V. The actual measurement of the voltage drop for the slotted case is 5.03 V. This indicates that the bubble induced voltage drop reduces for the slotted case by 0.3 V, which contributes to energy savings significantly. This value looks too high in comparison to the industrial cells, e.g. the total bubble induced voltage drop is only about 0.15-0.35 V [2]. As the current experiment is conducted at a small scale, the data should not be over interpreted.

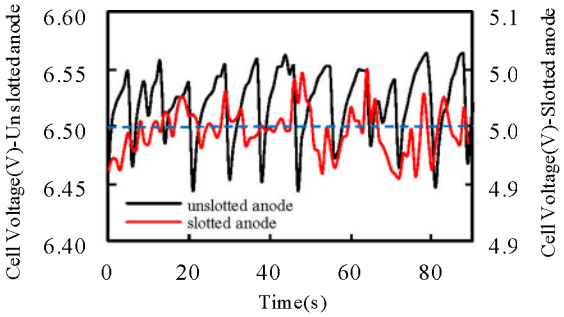

Figure 9 Cell voltage fluctuations against time on unslotted anode and slotted anode at current density of 0.9A/cm^2

In addition to the mean value, the effect of the slot can be clearly identified in Figure 9 in terms of the voltage fluctuation and the fluctuation frequencies. The voltage fluctuation for the unslotted case is higher than that of the slotted case, while the fluctuation frequency is much higher for the slotted cases. These

voltage drop patterns are consistent with bubble behavior shown in Figure 7. The bubbles are smaller and release more frequently for the slotted anode, thus the voltage fluctuation frequency increases. For the unslotted anode, the maximum bubble size is bigger, which contributes to a larger magnitude of voltage fluctuation.

The voltage fluctuation represents the difference in cell voltage with gas presence (high voltage) and gas release (low voltage). The mean fluctuation of voltage drop has been calculated by the following equation to quantify the difference between the unslotted and slotted anodes.

$$V_{fluctuation} = \frac{\sum_{m=1}^{M} |V_m - V_{ave}|}{M}$$

where $V_{fluctuation}$ is the average fluctuation of cell voltage, V_m refers the m^{th} cell voltage datum, and M is the total number of cell voltage points.

The average fluctuation of cell voltage decreases from 24.5 mV for the unslotted anode to 15.5 mV for slotted anode, which is about 36.7% reduction.

Figure 9 shows the slot technology is beneficial for reducing both bubble induced voltage drop and voltage fluctuation, which plays a positive role in energy saving and cell stability.

Cell Voltage vs Coverage. It is generally accepted that the fluctuation of cell voltage is mainly due to the gas release and the agitation of the bath-metal interface. It is impossible to describe the variation of bath-metal interface in this experiment, only the effect of gas release was investigated here.

In this section, the instantaneous gas coverage was calculated in the following equation using the image pixel information.

$$\varphi = \frac{\sum_{i=1}^{I} S_i}{a \times b}$$

where φ is the instantaneous coverage of a picture; I is the total number of bubbles in the picture; i refers the i^{th} bubble; S_i is the area of bubble i; a and b are the length and width of the anode bottom respectively.

Figure 10 displays the representative examples of bubble coverage and cell voltage fluctuation on the unslotted and slotted anodes at the fixed current density of 0.9 A/cm^2. It is interesting to note that the voltage drop and bubble coverage are closely correlated with a high voltage drop corresponding to a high bubble coverage. This indicated the cyclic release of bubbles at the anode bottom was one of the major reasons for the cell voltage fluctuation measured in industrial cells.

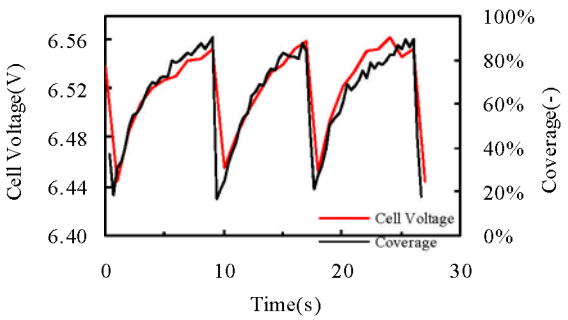

(a)

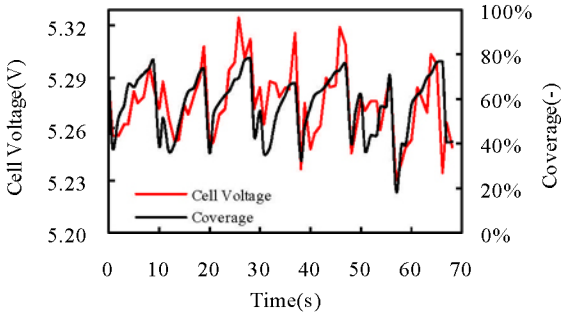

(b)

Figure 10 Gas coverage and cell voltage fluctuation against electrolysis time at current density of 0.9A/cm^2 on unslotted anode (a) and slotted anode (b)

For the unslotted anode, the coverage and its corresponding voltage curves fluctuate smoothly and regularity. On the other hand, the curves of slotted anode change violently, showing poor periodicity. The reason to this can be explained by the difference in bubble behavior on the two kinds of anodes: a) the maximum bubble size on the unslotted anode are much larger than that on slotted anode; b) the bubbles are more easily to escape from the slotted anode.

Current Density vs Bubble Coverage. For the bottom observation, the experiment was conducted at a range of current densities from 0.3 A/cm^2 to 1.3 A/cm^2. It is interesting to evaluate the effect of current density on the bubble coverage. The averaged gas coverage at different current densities was calculated based on the following equation.

$$\bar{\varphi} = \frac{\sum_{j=1}^{J} \varphi_j}{J}$$

where, $\bar{\varphi}$ is the average gas coverage for a series of pictures at a fixed current density; J is the total number of pictures at the current density; φ_j is the instantaneous coverage of picture j.

It is generally believed that the increase of current density results in a higher bubble coverage, which has been reported in previous studies (Fortin [1], Wang [3] and Alam [12]). However, as shown in Figure 11, the current experiment predicts an opposite trend. The maximum and averaged bubble coverage decreases when the current density increases for both unslotted and slotted anodes. The bath near the anode bottom receives more turbulence due to the faster gas generation rate at high current density, which may play a significant role for the quick release of bubbles from the bottom surface.

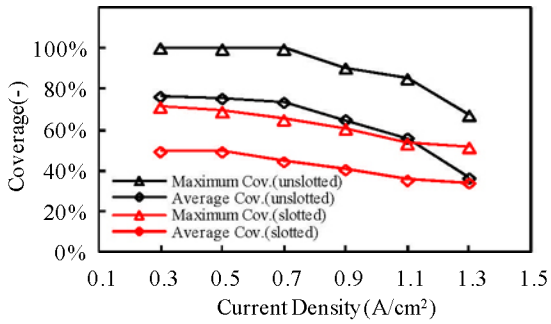

Figure 11 Maximum and averaged bubble coverage at different current densities for unslottted and slotted anodes

The bubble coverage on slotted anode is much lower than that on unslotted anode when the current density is less than 1.1 A/cm^2. At the highest current density performed in this experiment, e.g. 1.3 A/cm^2, the difference reduces. This is due to the significant reduction of the bubble coverage for the unslotted anode following the increase of the current density. If this is true, the benefit of slots will reduces for higher current densities. Further studies are necessary to fully clarify this issue in detail.

Conclusion

The bubble behavior in the Aluminum smelting process has been studied using laboratory transparent cells from both side and bottom observations.

The main findings of this study are:

1. The side observation in a single chamber cell showed that bubbles are released in a cyclic pattern. When the bubble grows to a size as large as the anode bottom surface and to a maximum thickness about 4 mm, it releases suddenly through the anode edge. The released bubble attaches to the anode side walls and rises quickly in the cell channel.
2. Bubble behavior in ACD has been observed in detail through a bottom observation in a double-chamber cell. Tiny bubbles were generated at the anode bottom surface in many spots. These tiny bubbles grew through diffusion of gases. The formation of large bubbles was mainly driven by coalescence of surrounding bubbles when their edges were connected.
3. The cell voltage is very consistent with the bubble coverage with a high voltage drop corresponding to a high bubble coverage. The gas coverage decreases with the increase of current density.
4. The anode slot affects the bubble behavior and resultant voltage drop significantly. With the presence of a 4 mm wide longitudinal slot, the mean bubble coverage reduces by about 38% and the maximum coverage by 33% at a current density of 0.9 A/cm^2. The bubble induced voltage drop and its fluctuation reduces consequently, with the mean fluctuation reduces by 36.7%.
5. The bubble coverage on the slotted anode was much lower than that on the unslotted anode when the current density was less than 1.1 A/cm^2. At the highest current density of 1.3 A/cm^2, performed in this experiment, the difference reduces.

Acknowledgements

The authors would like to thank the National Natural Science of China (51228401) for providing financial support. Zhibin Zhao also would like to thank the China Scholarship Council (CSC) for a visiting PhD scholarship to CSIRO.

Reference

1. S. Fortin, M. Gerhardt, and A.J. Gesing, "Physical Modeling of Bubble Behavior and Gas-release from Aluminum Reduction Cell Anodes," *Light Metals*, 1984, 721-741.
2. W.E. Haupin, "A Scanning Reference Electrode for Voltage Contours in Aluminum Smelting Cells," *Journal of Metals*, 23(10)(1971), 46-51.
3. X.W. Wang et al., "Development and Deployment of Slotted Anode Technology at Alcoa," *Light Metals*, 2007, 539-544.
4. S. Das et al., "Principal Characteristics of a Bubble Formation on a Horizontal Downward Facing Surface," *Colloids and surface A: Physicochem. Eng. Aspects*, 411(2012), 94-104.
5. Y. Liu et al., "Research on the Penetration Depth in Aluminum Reduction Cell with New Type of Anode and Cathode Structures," *Journal of Metals*, 66(7)(2014), 1202-1209.
6. L.I. Kiss, S. Poncsak, and J. Antille, "Simulation of the Bubble Layer in Aluminum Electrolysis Cells," *Light Metals*, 2005, 559-564.
7. A. Perron, L.I. Kiss, and S. Poncsak, "Regimes of the Movement of Bubbles under the Anode in an Aluminum Electrolysis Cell," *Light Metals*, 2005, 565-570.
8. K.Y. Zhang et al., "Computational Fluid Dynamics (CFD) Modeling of Bubble Dynamics in the Aluminum Smelting Process," *Industrial & Engineering Chemistry Research*, 52(33)(2013), 11378-11390.
9. K.X. Qian, Z.D. Zhang, and J.J.J. Chen, "Bubble Coverage and Bubble Resistance Using Cells with Horizontal Electrode," *Journal of Applied Electrochemistry*, 28(1998), 1141-1145.
10. J.J.J. Chen, K.X. Qian, and J.C. Zhao, "Resistance Due to the Presence of Bubbles in an Electrolytic Cell with a Grooved Anode," *IChemE.*, 79(2001), 383-388.
11. Y.Q. Xue, N.J. Zhou, and S.Z. Bao, "Normal Temperature Analogue Experiment of Anode Bubble's Behavior in Aluminum Electrolysis Cells," *The Chinese Journal of Nonferrous Metals*, 16(2006), 1823-1828.
12. M. Alam et al., "Investigation of Anodic Gas Film Behavior in Hall–Heroult Cell Using Low Temperature Electrolyte," *Metallurgical and Materials Transactions B.*, 44(2013), 1155-1165.
13. M.A. Cooksey, and W. Yang, "PIV Measurements on Physical Models of Aluminium Reduction Cells," *Light Metals*, 2006, 359-365.
14. K.Y. Zhang et al., "Numerical Investigation of Bubble Dynamics in Aluminium Electrolytic Cells," *Light Metals*, 2012, 881-886.
15. Y.Q. Feng, M.A. Cooksey, and P. Schwarz, "CFD Modeling of Electrolyte Flow in Aluminium Reduction Cells," *Light Metals*, 2007, 339-344.
16. N.J. Zhou, X.X Xia, and S.Z. Bao, "Effect of Electromagnetic Force and Anode Gas on Electrolyte Flow in Aluminum Electrolysis Cell," *Journal of Central South University of Technology* , 13(5)(2006), 496-500.
17. W.E. Haupin, and W.C. McGrew, "See-Through Hall–Héroult cell," *Aluminium*, 51(1975), 273-275.
18. Z.X. Qiu, L.M. Fan, and K. Grjotheim, "Dissolution of Aluminum in Cryolite-alumina Melts (See-Through Cell Studies)," *Light Metals*, 1986, 525-533.
19. Z.X. Qiu et al., "Formation of Metal Fog During Molten Salt Electrolysis Observed in a See-Through cell," *Journal of Applied Electrochemistry*, 17(1987), 707-714.
20. J.L. Xue, and H.A. Oye, "Bubble Behavior-Cell Voltage Oscillation During Aluminum Electrolysis and the Effects of Sound and Ultrasound," *Light Metals*, 1995, 265-271.
21. B.L. Gao et al., "Study on Bubble Behavior on Anode in Aluminum Electrolysis - Part II," *Light Metals*. 2006, 467-470.
22. T. Utigard, and J.M. Toguri, "Anode Gas Behavior During Electrolysis," *Light Metals*, 1986, 405-413.
23. L. Cassayre et al., "Gas Evolution on Graphite and Oxygen Evolving Anodes During Aluminum Electrolysis," *Light Metals*, 2006, 379-383.